J. of Korean Oil Chemists' Soc.,
Vol. 13. No. 3, Nov., 1996. 1~14

〈總 說〉

Novel Concepts of the Aggregation Structure of Fatty Acid Monolayers on the Surface of Water

Tisato Kajiyama and Taishi Kuri

Dept. of Chemical Science and Technology, Kyushu University

Introduction

Langmuir-Blodgett (LB) films have been applied to molecular electronics, nonlinear optics, and biosensors. Their useful properties can be accessed by using a defect-free monolayer—the precursor of LB films. In order to prepare a defect-free or defect-diminished monolayer, it is necessary to estimate the molecular arrangements and structural defects in the monolayer. The actual structure of monolayers on the surface of water have been proposed on the basis of recent morphological and structural studies.[1-7] Molecular-aggregation processes or monolayer-formation processes do not always match the general concept[8] concluded from surface pressure-area (π-A) isotherms. Therefore, a universal understanding has not been reached. Here we present a novel and systematic classification for the aggregation structure of monolayers on the water surface and also demonstrate how to prepare defect-diminished monolayers.

Evaluation of Melting and Crystalline Relaxation Temperatures of Fatty-Acid Monolayers on the Surface of Water

Benzene solutions of fatty acids spread on top of water to form monolayers. The subphase temperature T_{sp} was varied in a temperature range of 274–321 K by circulating constant-temperature water around an aluminum support of a trough. Pressure-area (π-A) isotherms were obtained at various T_{sp} values with a microprocessor-controlled film balance system. The static elasticity K_S of the monolayer on the water surface was evaluated from the negative slope of the π-A isotherm.[1] Figure 1 shows the π-A (solid line) and the log K_S-A (broken line) isotherms for the stearic-acid monolayer at T_{sp} of 293 K. Log $K_{S(max)}$ was defined as the maximum of log K_S which corresponded to the value at the collapsing point. At this point, although the col-

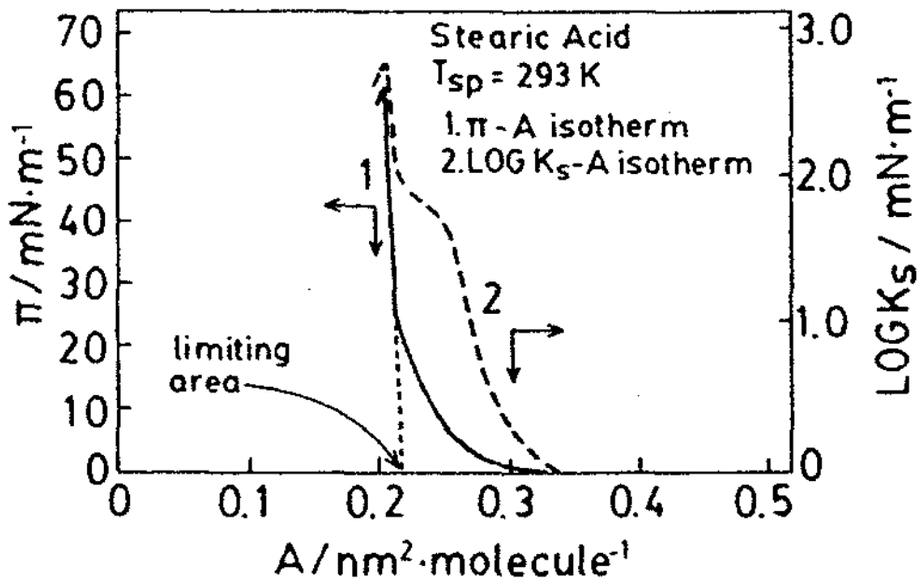

Figure 1. π-A and log K_s-A isotherms of stearic-acid monolayer at T_{sp} of 293 K.

lapsed monolayer fragments were observed as a patchy pattern on the base monolayer (the substrate monolayer on the water surface), molecules in the base monolayer were packed most densely and homogenously. Therefore, it is reasonable to consider that the homogenous compression force was transmitted throughout the monolayer. Then, the temperature dependence of log $K_{S(max)}$ was adopted for determination of the melting temperature T_m, as well as the crystalline relaxation temperature T_{α_c} of the monolayer on the water surface.

The hydrophilic SiO substrate (static water contact angle of 30°) was prepared by vapor-depositing SiO onto a Formvar substrate, with which an electron microscope grid (200-mesh) was covered.[9] Electron-microscopy observations were carried out at the same temperature as the T_{sp} at which the monolayer was prepared on the water surface. The hydrophilic part of the monolayer touches the substrate surface in the upward drawing method. The crystallographic structure of the monolayer was dependent on the hydrophilic or hydrophobic characteristics of the substrate, perhaps because of the difference of interfacial interaction. The monolayer that was transferred to a hydrophilic substrate such as SiO showed that the crystal system of the monolayer was hexagonal. This hexagonal crystal system matches that of the arachidic-acid monolayer on the water surface; this was confirmed by grazing-incidence in-plane x-ray diffraction.[5] Since the hydrophilic group of the monolayer touches the hydrophilic SiO substrate during transfer of the monolayer, this interfacial condition is similar to that of the monolayer on the water surface with respect to the magnitude of interfacial free energy between the hydrophilic (polar) group of the monolayer and the hydrophilic substrate surface. Therefore, it is reasonable to consider that the hexagonal crystal system of the monolayer on the water surface can be transferred and stably maintained on the hydrophilic substrate. In order to investigate the thermal behavior of the monolayer structure on the water surface, we transferred the monolayer onto the hydrophilic SiO substrate by the upward drawing method with a drawing speed of 60 mm min^{-1} at various T_{sp} values and at a certain surface pressure where each monolayer was morphologically homogenous.[10]

Figure 2 shows the T_{sp} dependence of log $K_{S(max)}$ for a stearic-acid monolayer on the water surface, as well as the electron-diffraction (ED) patterns of the monolayer transferred onto a hydrophilic substrate at a surface pressure of 20 mN m^{-1}. The ED patterns were taken at the T_{sp} at which the monolayer was prepared. The magnitude of log $K_{S(max)}$ started to decrease at approximately 298 K and 317 K. The ED patterns at 313 K and 319 K were a crystalline Debye ring and an amorphous halo, respectively. Therefore, Figure 2 indicates that a fairly remarkable decrease of log $K_{S(max)}$ at around 317 K corresponds to the melting behavior of the stearic-acid monolayer on the water surface. Also, melting temperatures of myristic-, palmitic-, and arachidic-acid monolayers on the water surface were similarly estimated to be 278 K, 301 K and 331 K, respectively, on the basis of the T_{sp} dependence of log $K_{S(max)}$ and ED patterns. The melting temperatures of the fatty-acid monolayers are much lower than those of corresponding three-dimensional crystals because the monolayers are thermodynamically less stable than the three-dimensional crystals. However, the magnitude difference between T_m for monolayer and bulk crystal becomes smaller with an increase in alkyl chain length. This indicates that the intermolecular aggregation force in the monolayer state increases with increasing alkyl chain length.[11]

Figure 2 also shows that the slope of log $K_{S(max)}$ versus T_{sp} curve for the stearic-acid monolayer slightly decreased at approximately 298 K which is denoted by

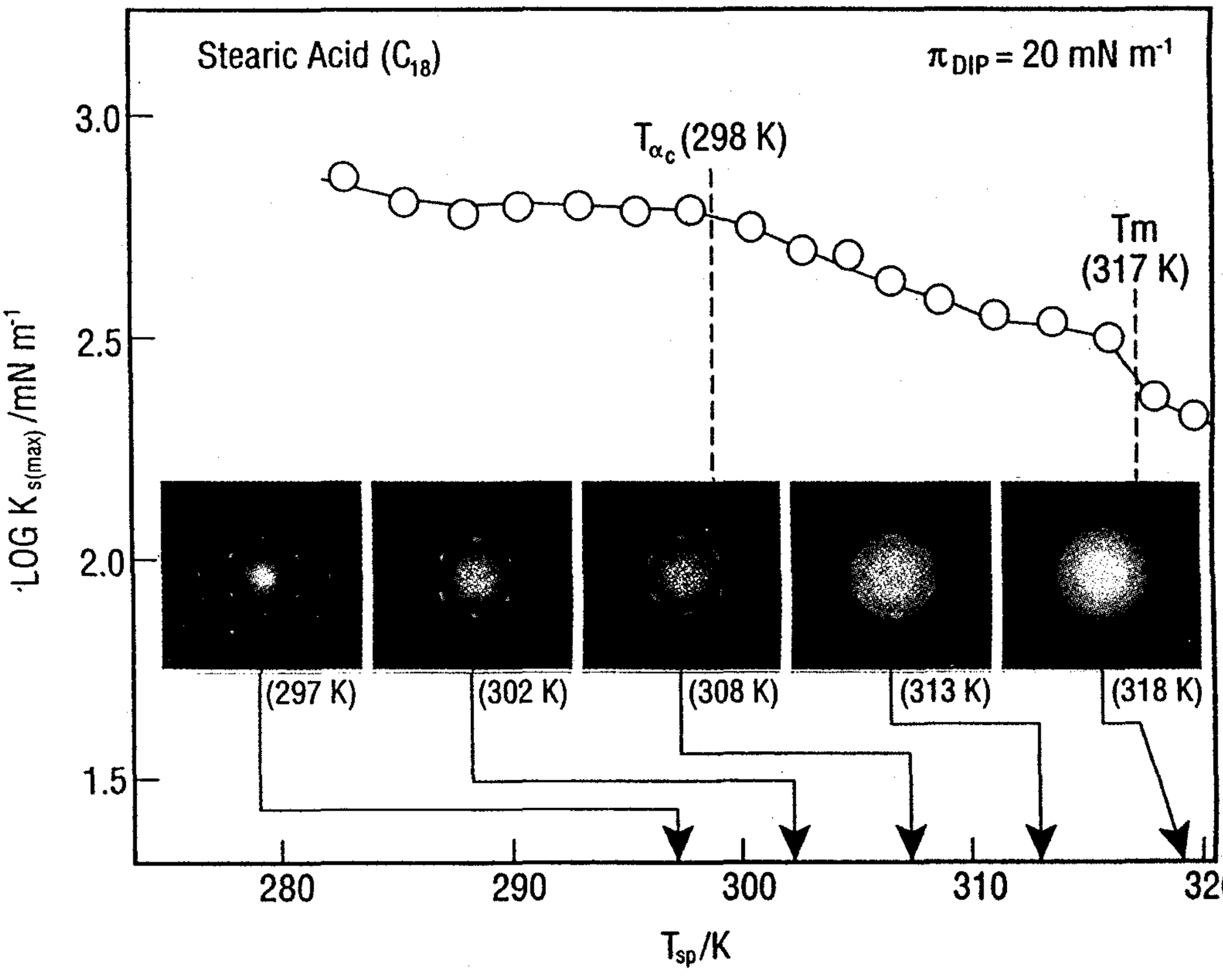

Figure 2. T_{sp} dependence of log $K_{s(max)}$, and electron-diffraction patterns of stearic-acid monolayers.

T_{α_c}. In a T_{sp} range below 298 K, the ED pattern of the stearic-acid monolayer exhibited sharp crystalline spots with spacings of 0.42 and 0.24 nm. Since the ratio of reciprocal spacings is $1:\sqrt{3}$, stearic-acid molecules are packed in a hexagonal unit cell. These diffraction spots were assigned to (10) and (11) reflections, respectively. In contrast, in a T_{sp} range above 298 K, the ED spots tended to be more arced along an azimuthal direction and broader with an increase of T_{sp}, finally resulting in the Debye ring. This indicates that the orientation of stearic-acid molecules and/or crystalline domains becomes broader or less regular with an increase in T_{sp} above approximately 298 K. The (10) spacing versus T_{sp} curve exhibited a distinct break at approximately 298 K. Thus, the temperature range of the break point on the (10) spacing versus T_{sp} curve apparently corresponds to that for an apparent decrease of log $K_{S(max)}$ as shown in Figure 2. The T_{sp} dependence of log $K_{S(max)}$ and the (10) spacing are very similar to that of the mechanical crystalline relaxation mechanisms which were extensively studied for single-crystal mats and spherulitic films of high-density polyethylene (PE).[12,13] The lateral attractive force between PE chains in the crystal lattice is weaker than the covalent bonding force along a PE chain. Therefore, the rotational oscillation around a PE chain readily occurs across the intermolecular-energy barrier in a higher temperature range at which the oscillations of neigh-

boring chains are incoherent. This causes an increase of anharmonicity for intermolecular potential energy, which was confirmed by an increase in the Grüneisen constant evaluated from the pressure dependence of sound velocity and compressibility.[14,15] Therefore, a remarkable increase in anharmonicity on intermolecular potential energy causes an increase in the viscous contribution to the viscoelastic characteristics in a crystalline region and also an apparent change in the thermal expansion of the lattice spacing. These viscoelastic characteristics in a crystalline region were designated "crystalline relaxation behavior." Consequently, it is reasonable to conclude from the T_{sp} dependences of log $K_{S(max)}$ and the (10) spacing that the viscoelastic crystalline relaxation behavior was confirmed for the first time even in the crystalline fatty-acid monolayers.

Morphological and Structural Studies of Crystalline and Amorphous Monolayers on the Water Surface

Figure 3a shows the π-A isotherm for the palmitic-acid monolayer spread on the water surface at T_{sp} of 283 K below T_m of 301 K and the bright-field images and the ED patterns of the monolayers which were transferred onto the hydrophilic SiO substrate. The π-A isotherm showed a sharp rise of surface pressure with decreasing surface area without any appearance of a plateau region. The limiting area and collapse pressure for the palmitic-acid monolayer were 0.23 nm^2 $molecule^{-1}$ and 54 mN m^{-1}, respectively. At 0 mN m^{-1}, many isolated domains were observed in a bright-field image. The bright-field image of the monolayer transferred at 20 mN m^{-1} exhibited a fairly uniform, smooth, and continuous morphology. Also, the bright-field image at 30 mN m^{-1} showed heterogenous aggregation which was composed of partially patched domains because of the collapse of the monolayer. The ED pattern of the palmitic-acid monolayer transferred at 0 mN m^{-1} exhibited a crystalline Debye ring. Therefore, the monolayer domains observed in the bright-field image at 0 mN m^{-1} were in a crystalline state and their crystallographic axes were oriented randomly. On the other hand, the ED patterns at 20 and 30 mN m^{-1} showed crystalline hexagonal spots. This indicates that crystalline domains in a fairly wide area were fused or recrystallized at the interface because of sintering behavior caused by higher surface pressure, resulting in the formation of a large-area monodomain monolayer. It has been confirmed from synchrotron x-ray diffraction studies that lead-stearate[16] and arachidic-acid[5] monolayers were in a crystalline state at every surface pressure as well as 0 mN m^{-1} at T_{sp} of 293 K below T_m of the monolayer on the water surface. Therefore, the bright-field images and the ED patterns in Figure 3a reveal that two-dimensional crystalline domains were grown immediately after spreading a solution on the water surface and were also gathered during a process of surface compression. Finally, all crystalline domains in a fairly wide area formed crystallographically homogenous single crystals. The monolayer as shown in Figure 3a was designated the "fusion-oriented crystalline monolayer."[17]

On the other hand, at T_{sp} of 293 K above T_{α_c} below T_m of the palmitic-acid monolayer, a surface pressure-induced crystallographic orientation was not observed even at higher surface pressure.[18] Since the crystalline relaxation process corresponds to a change from elastic to viscoelastic characteristics in a crystalline phase because of a considerable contribution of anharmonic thermal molecular vibration, sintering among crystalline domains at T_{sp} above T_{α_c} prevented by the anharmonic thermal molecular vibration, resulting in random orientation of crystalline domains along their crystallographic axes. This type of monolayer was designated the "randomly assembled crystalline monolayer."

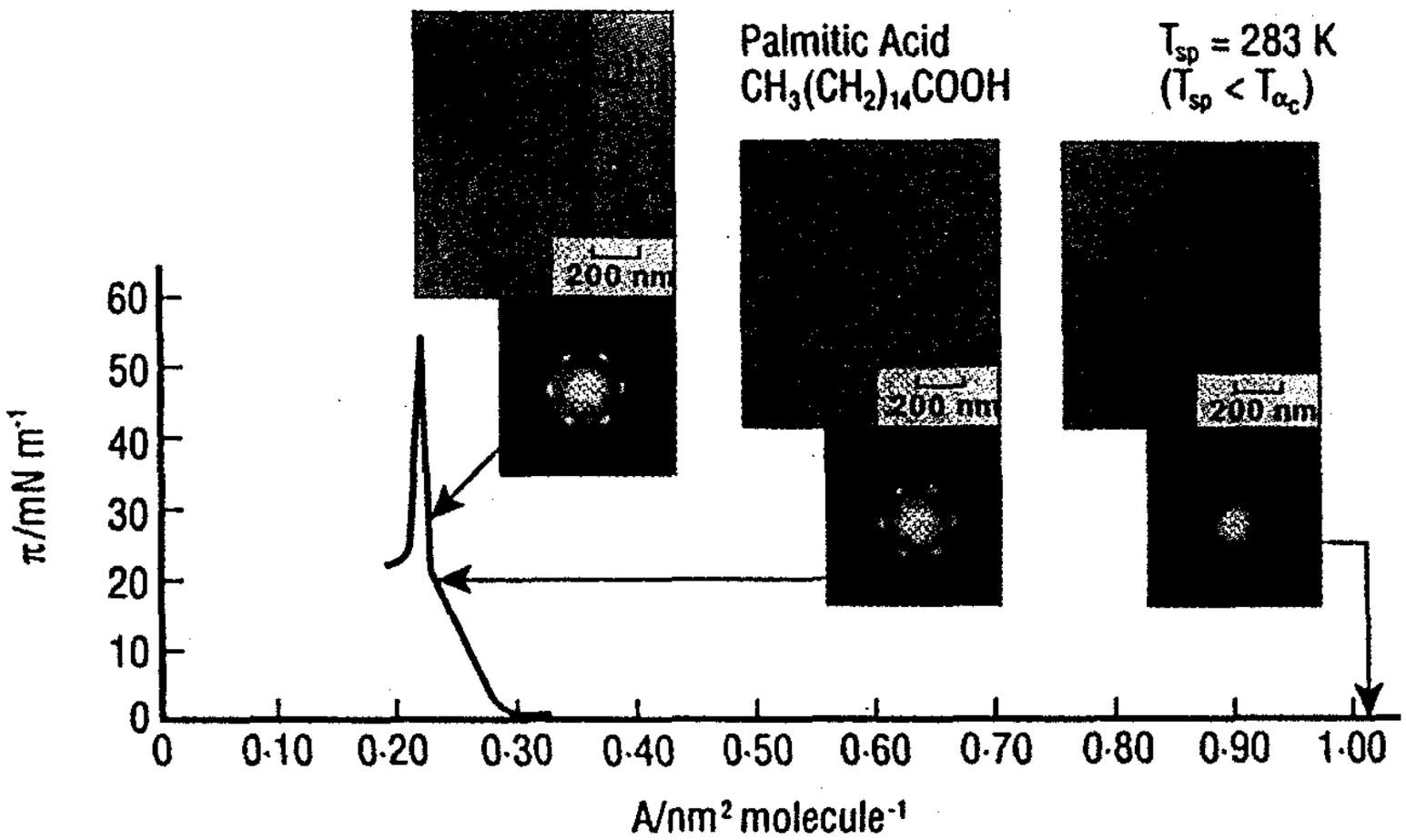

Figure 3. π-A isotherms, electron micrographs, and ED patterns of palmitic-acid monolayer at (a) T_{sp} of 283 K and (b) T_{sp} of 303 K.

Figure 3b shows the π-A isotherm for the palmitic-acid monolayer spread on the water surface at T_{sp} of 303 K above T_m of the monolayer. A plateau region of the π-A isotherm was observed in a range of 0.35–0.50 nm^2 $molecule^{-1}$. The limiting area and the collapse pressure for the monolayer were 0.28 nm^2 $molecule^{-1}$ and 38.0 mN m^{-1}, respectively. These values of the limiting area and the collapse pressure were larger and smaller, respectively, than those for the crystalline palmitic-acid monolayer shown in Figure 3a. The bright-field image and the

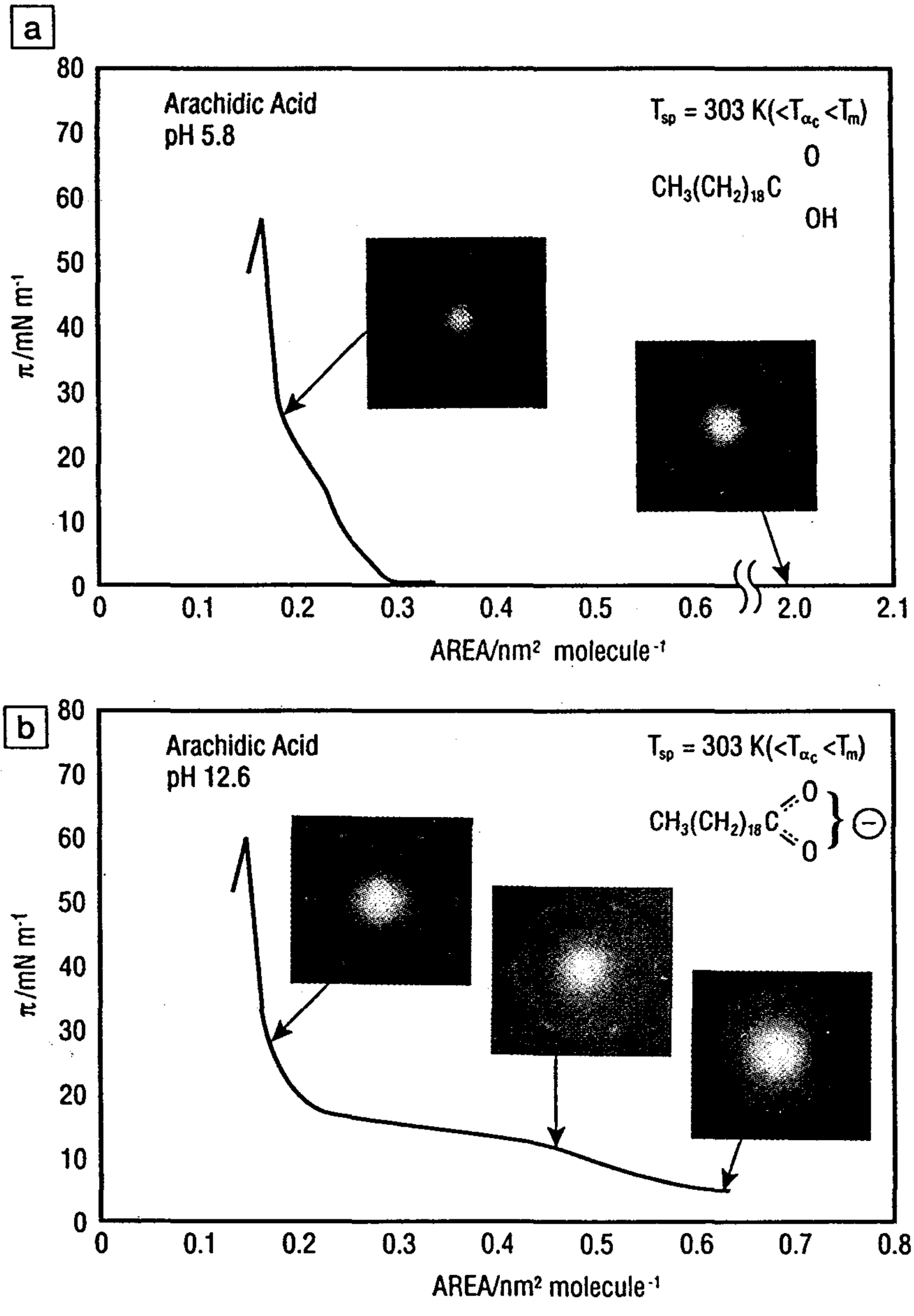

Figure 4. π-A isotherms and ED patterns of arachidic-acid monolayers at a T_{sp} of 303 K on the water subphase of (a) pH 5.8 and (b) pH 12.6.

ED pattern of the monolayer even at a surface pressure of 0 mN m^{-1} showed island fragments and an amorphous halo, respectively. The bright-field images clearly showed the aggregation process of these domains and the appearance of partial collapse with an increase in surface pressure, whereas each ED pattern remained an amorphous halo. Thus, Figure 3b indicates that amorphous do-

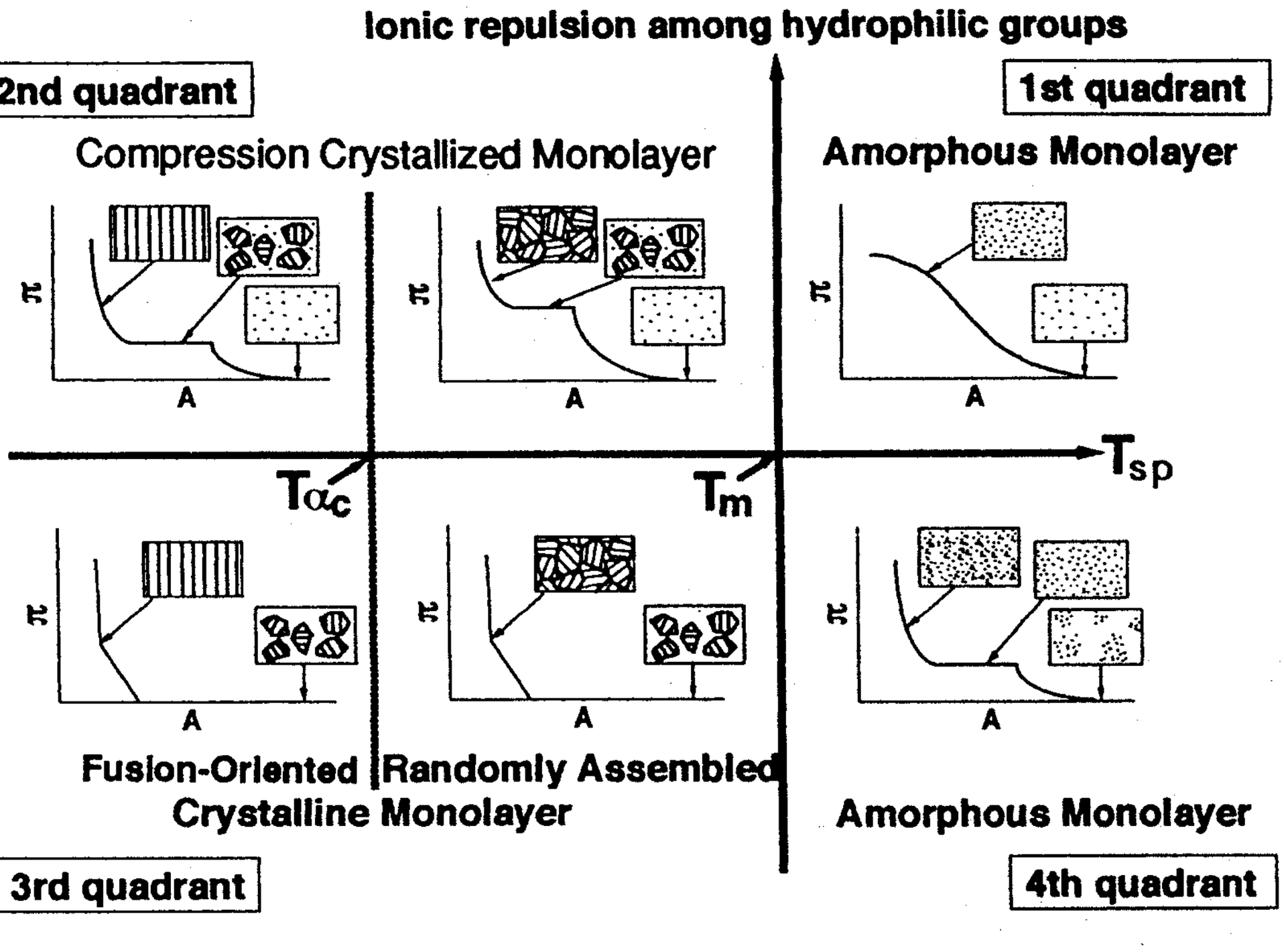

Figure 5. Classification of the aggregation structure of fatty-acid monolayers on the water surface.

mains, which formed immediately after spreading a solution on the water surface, aggregate into a large amorphous monolayer during compression. Although the monolayer was compressed up to the collapsing pressure at T_{sp} above T_m, the monolayer was still in an amorphous state without pressure-induced crystallization. This type of monolayer was designated an "amorphous monolayer."[2]

The Effect of Ionic Repulsion Among Hydrophilic Groups on the Aggregation Structure of Monolayers

Arachidic-acid monolayers were prepared from a benzene solution on water subphases of pH 5.8 (pure water) and 12.6 (adjusted by the addition of NaOH) at T_{sp} of 303 K below T_m(328 K) of the monolayer.[19] The ionic dissociation state of the hydrophilic group was estimated on the basis of the stretching vibrations of carbonyl and carboxylate groups by Fourier transform-infrared attenuated total reflection (FT-IR ATR) measurements. Seventy arachidic-acid monolayers were transferred on a germanium ATR prism. Infrared-absorption measurements revealed that most carboxylic groups of arachidic-acid molecules did not dissociate on the water subphase of pH 5.8, whereas all carboxylic groups dissociated as carboxylate ions on the water subphase of pH 12.6.

Figures 4a and b show the π-A isotherms for the arachidic-acid monolayers on the water surface of pH 5.8 (pure water) and of pH 12.6, respectively, at T_{sp} of 303 K. In the case of a neutral state of arachidic acid (pH 5.8), the π-A isotherm showed a sharp rise of surface pressure with decreasing surface area without any

appearance of plateau region. The ED patterns at surface pressures of 0 and 25 mN m^{-1} showed crystalline arcs and crystalline spots, respectively, indicating the formation of a "crystalline monolayer." In the case of a dissociated state of arachidic acid on the water subphase of pH 12.6 at T_{sp} of 303 K, a plateau region of the π-A isotherm was observed in a range of 0.3–0.5 nm^2 $molecule^{-1}$ as shown in Figure 4b. The ED pattern at 5 mN m^{-1} showed an amorphous halo, whereas those at 12 and 28 mN m^{-1} exhibited crystalline arcs or spots, respectively. Therefore, Figure 4b indicates that the arachidic-acid monolayer is crystallized by compression on the water surface of pH 12.6. This type of monolayer has been classified as the "compression crystallized monolayer" or the "pressure-induced crystallized monolayer."[7,17]

Figure 5 shows the classification of fatty-acid monolayers based on the aggregation structure with respect to thermal (T_{sp}, T_{α_c}, T_m) and chemical (the degree of ionic dissociation of hydrophilic group) factors. This figure is divided into the four quadrants by the two axes of T_{sp} and the repulsive force among hydrophilic groups. In the case of amphiphiles with nonionic hydrophilic groups (corresponding to the third and fourth quadrants), isolated domains grown immediately after spreading a solution on the water surface are gathered to form a morphologically homogenous monolayer by compression. Then, at T_{sp} below T_m (the third quadrant), the monolayer is in a crystalline phase which is designated "the crystalline monolayer." The crystalline monolayer is further classified into two types: (1) crystalline domains assembled into a large homogenous crystalline monolayer because of compression-induced sintering at the interfaces of monolayer domains at T_{sp} below the crystalline relaxation temperature (T_{α_c}) and (2) crystalline domains without any special orientation among domains at T_{sp} above T_{α_c}. At T_{sp} above T_m (the fourth quadrant), the monolayer is in an amorphous phase which is designated the "amorphous monolayer." In the case of amphiphiles with ionic hydrophilic groups (the first and second quadrants), a distinct domain structure is not formed at a lower surface pressure owing to the electrostatic repulsion among polar head groups. At T_{sp} below T_m (the second quadrant), amphiphile molecules form a large homogenous crystallized monolayer ($T_{sp} < T_{\alpha_c}$) or an assembly of crystallized domains ($T_{\alpha_c} < T_{sp} < T_m$) owing to the contribution of van der Waals forces through a gas or a liquid phase with an increase of surface pressure. On the other hand, at T_{sp} above T_m (the first quadrant), the monolayer is not crystallized by compression because of fairly active thermal molecular motion.[17]

Construction of Defect-Diminished Crystalline Monolayers

A benzene solution of stearic acid of 3.5×10^{-3} mol l^{-1} was prepared as a spreading solution. Scheme 1 shows the preparation process for a cooling-crystallized monolayer. The amorphous monolayer was prepared on the pure water surface at T_{sp} of 320 K above T_m of 317 K and then was compressed to a surface pressure of 15 mN m^{-1}. While maintaining the surface pressure at 15 mN m^{-1}, T_{sp} was reduced to 303 K below T_m at a rate of 40 K h^{-1}. Then the monolayer was further crystallized for 3 h on the water surface. This monolayer was again compressed to a surface pressure of 26 mN m^{-1}, at which point the stearic-acid monolayer was confirmed to be morphologically homogenous.[2,10] The monolayer constructed by this method was designated the "cooling-crystallized monolayer." The crystallographical distortion (D_{lat}) and crystallographical continuity (L_{lat}) of the cooling-crystallized monolayer were compared with those of the crystalline monolayer. The magnitudes of D_{lat} and L_{lat} were evaluated by a modified single line method based on Fourier

Table I: Crystallographical Distortion and Continuity for Crystalline and Crystallized Monolayers.

	Crystallographical Distortion, D_{lat}/%	Crystallographical Continuity, L_{lat}/nm
Crystalline monolayer (26 mN/m, 293 K)	4.9	6.4
Cooling-crystallized monolayer (15 mN/m, 303 K)	1.5	1.2×10^2
Polyethylene (Single-crystal)	<2.0	30 ~ 60

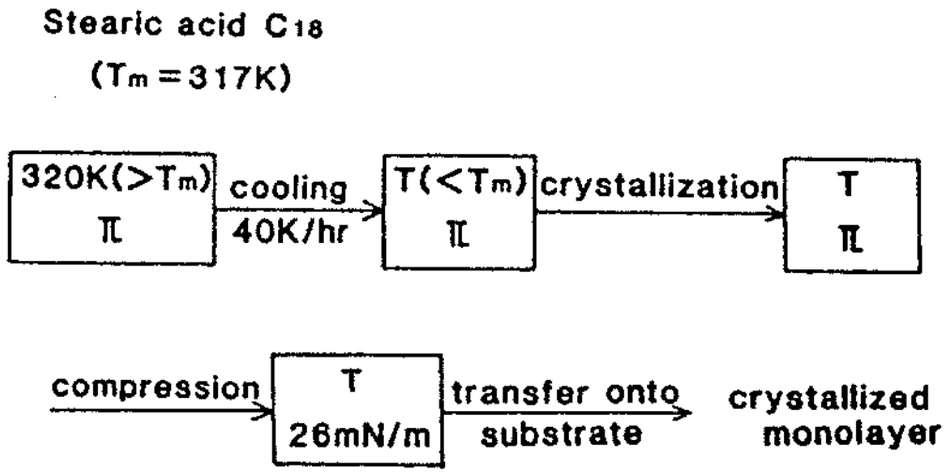

Scheme 1. Flow sheet for construction of a cooling-crystallized monolayer.

Spreading monolayer on the water surface
↓ Compression (120 $mm^2 \cdot sec^{-1}$)
Area-creep (10 $mN \cdot m^{-1}$)
↓ Compression (6 $mm^2 \cdot sec^{-1}$)
Area-creep (13 $mN \cdot m^{-1}$)
↓ Compression (6 $mm^2 \cdot sec^{-1}$)
Area-creep (15 $mN \cdot m^{-1}$)
↓ Compression (6 $mm^2 \cdot sec^{-1}$)
Area-creep (17 $mN \cdot m^{-1}$)
↓ Compression (6 $mm^2 \cdot sec^{-1}$)
Area-creep (18.5 $mN \cdot m^{-1}$)
↓ Compression (6 $mm^2 \cdot sec^{-1}$)
Area-creep (20 $mN \cdot m^{-1}$)
↓ Compression (6 $mm^2 \cdot sec^{-1}$)
Area-creep (21.5 $mN \cdot m^{-1}$)
↓ Compression (6 $mm^2 \cdot sec^{-1}$)
Area-creep (23 $mN \cdot m^{-1}$)
↓
Transferred onto hydrophilic SiO substrate

Scheme 2. Flow sheet for preparation of a monolayer by the multistep creep method.

analysis of ED profiles.[20,21] Table I shows the values of D_{lat} and L_{lat} for crystalline and cooling-crystallized monolayers of stearic acid. Though the magnitude of D_{lat} for the cooling-crystallized monolayers is comparable to that of high-density PE single crystals or spherulite, L_{lat} is 5–8 times as large as that of high-density PE.[13] Therefore, Table I indicates that cooling crystallization of an amorphous monolayer on the water surface is remarkably effective for constructing a two-dimensional crystallized monolayer with significant crystallographical continuity and a small fraction of crystalline defects.

Scheme 2 shows the preparation process of the stearic-acid monolayer by the multistep creep method.[22] The stearic-acid monolayer was compressed to a surface pressure of 10 mN m^{-1}. The variation of the monolayer area was measured with creep time while maintaining the surface pressure at 10 mN m^{-1}. The monolayer was then further compressed to 13 mN m^{-1} and again, the monolayer was maintained at 13 mN m^{-1} to measure its area-creep behavior. Stepwise, the monolayer was finally compressed to 23 mN m^{-1}. Figure 6 shows the area-creep behavior and bright-field images of the stearic-acid crystalline monolayers prepared by the multistep creep method and the conventional continuous compression method to 23 mN m^{-1}. In the case of the continuous com-

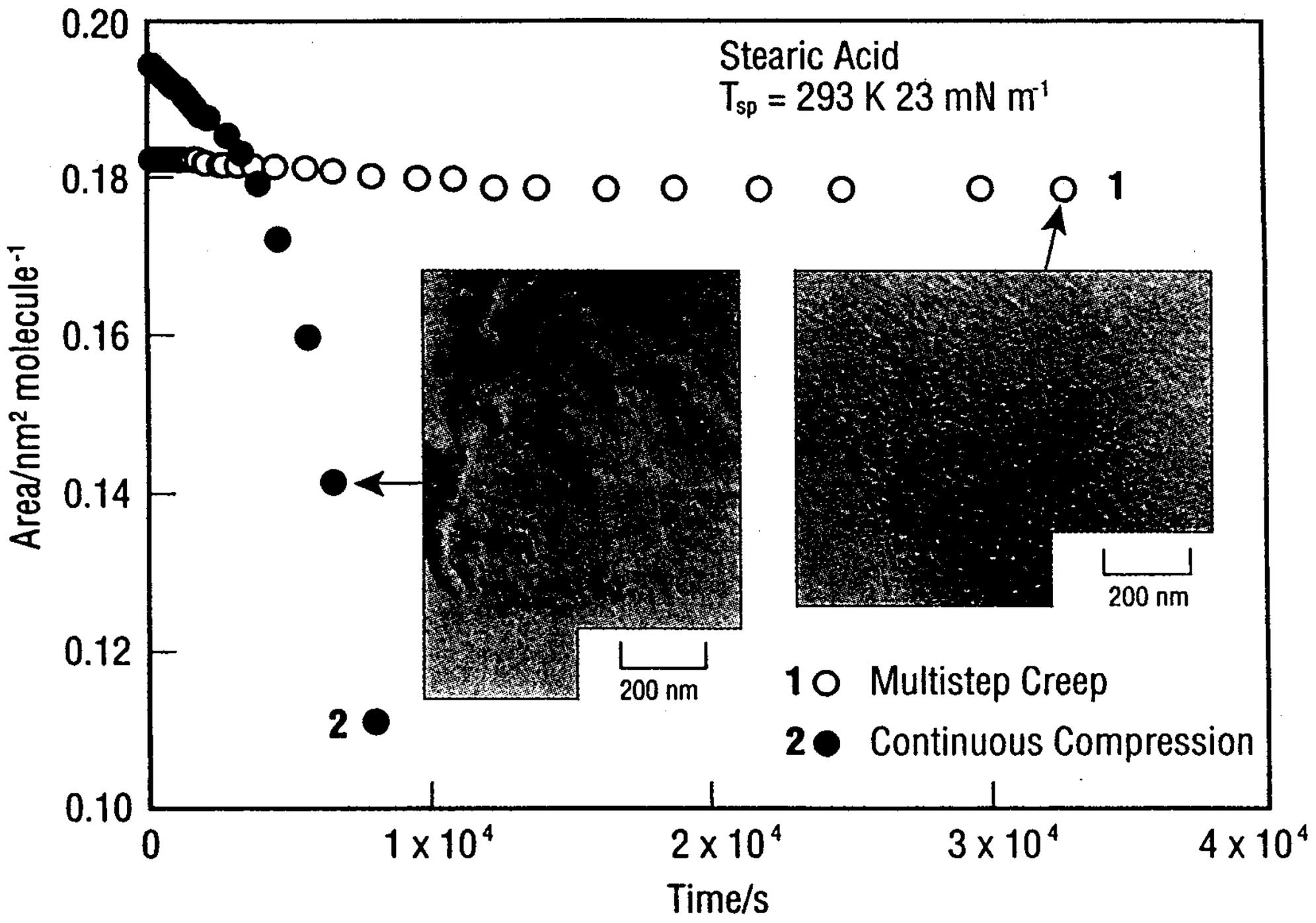

Figure 6. Area-creep behavior and bright-field images of stearic-acid crystalline monolayers prepared at 23 mN m^{-1} by the multistep creep and continuous compression methods.

pression method, the surface area of the monolayer decreased remarkably with creep time and the monolayer morphology was heterogenous after the area creep. Hence, it is possible to ascribe this remarkable decrement of the surface area to the localized collapse of the monolayer. In contrast, the surface area of the monolayer which was prepared by the multistep creep method decreased very slightly with creep time and remained almost constant after long-time area-creep. The magnitude of surface area after the multistep creep was comparable to that of the calculated surface area on the basis of its ED profile, indicating the close packing of molecules in the monolayer. Further, the electron micrographs of the monolayer that was prepared by the multistep creep method showed that the monolayer was still morphologically homogenous after the long-time area creep at 23 mN m^{-1}. Thus, the multistep creep method produces a crystalline monolayer which is not collapsed even after long-time area-creep at high surface pressure.

Direct Observation of Molecular Arrangements in Fatty-Acid Monolayers with an Atomic Force Microscope

Figure 7a shows an atomic force microscopy (AFM) image for a lignoceric-acid monolayer on a scan area of 13.5 × 13.5 nm^2. The fast Fourier transform (FFT) spectrum of the AFM image revealed that the brighter portions in Figure 7a were arranged in a hexagonal array with a (10) spacing of 0.43 nm. This

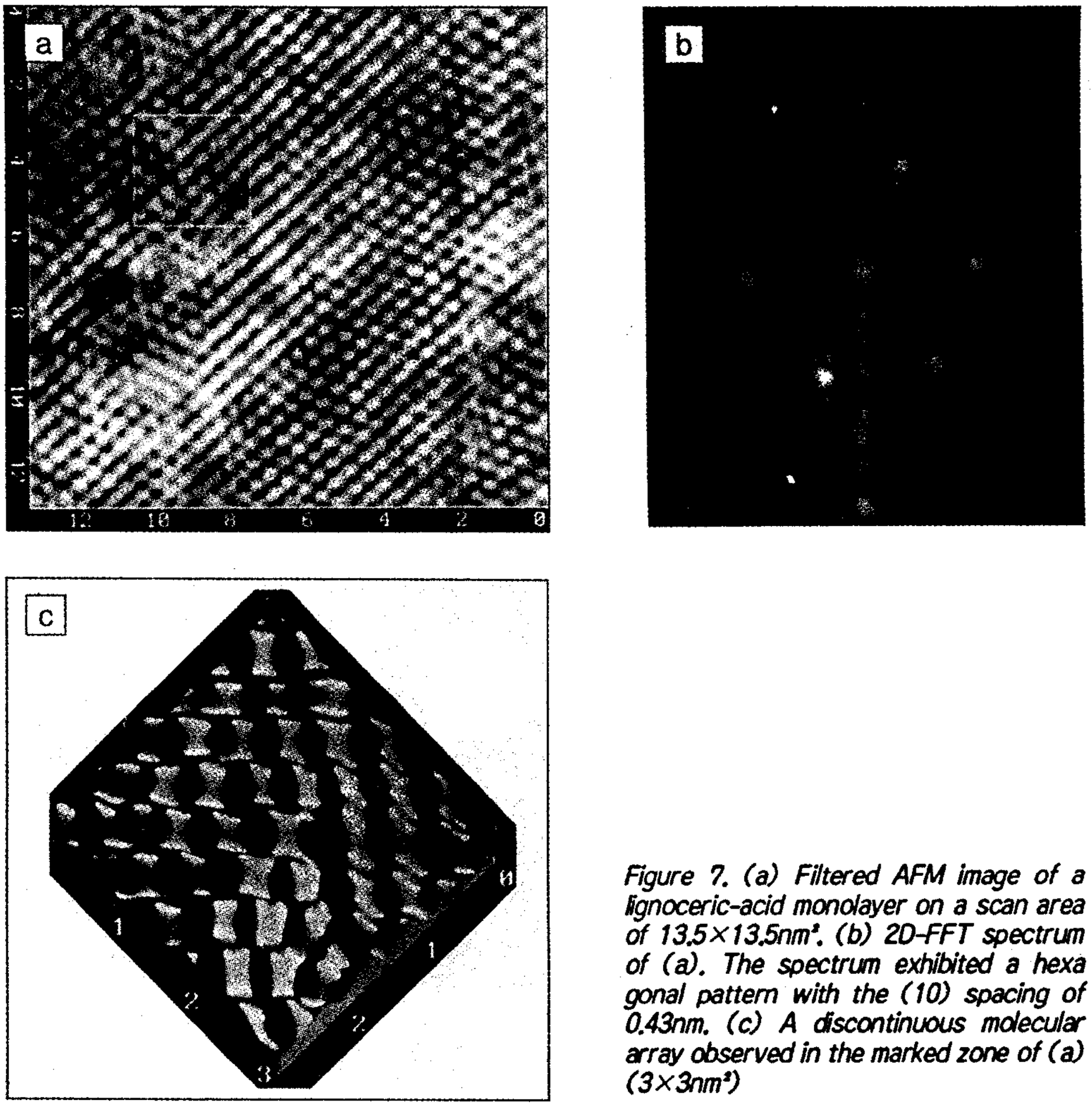

Figure 7. (a) Filtered AFM image of a lignoceric-acid monolayer on a scan area of 13.5×13.5nm². (b) 2D-FFT spectrum of (a). The spectrum exhibited a hexa gonal pattern with the (10) spacing of 0.43nm. (c) A discontinuous molecular array observed in the marked zone of (a) (3×3nm²)

magnitude matches the spacing of 0.43 nm which was estimated from the ED pattern of the lignoceric-acid monolayer and also is quite different from the 0.46 nm spacing of a mica substrate. It is therefore reasonable to conclude that the brighter portions in the AFM image represent the individual methyl groups of the lignoceric-acid molecules in the monolayer and also that lignoceric-acid molecules are regularly packed with a hexagonal array. The periodic hexagonal array extended over ~10 nm.[22-24]

Figure 7b shows the two-dimensional (2D) FFT spectrum of the image shown in Figure 7a. The bright spots in the 2D-FFT spectrum exhibit a hexagonal pattern with (10) spacing of 0.43 nm. The magnitude of the (10) spacing matches well with the spacing of 0.43 nm which was estimated from the ED pattern of the lignoceric-acid monolayer.[19] Moreover, the occupied area of a lignoceric-acid molecule in the monolayer that was evaluated from the AFM image and the ED pattern was 0.21 nm^2 $molecule^{-1}$. This magnitude was close to 0.25 nm^2 $molecule^{-1}$ being evaluated on the basis of π-A isotherm measurements. Therefore, Figures 7a and b show that

lignoceric-acid molecules are regularly arranged in a hexagonal array. A regularly periodic hexagonal array in the AFM image was extended over about 10 nm. This magnitude of the periodic hexagonal array was comparable to the magnitude of crystallographical continuity which was evaluated by a single line method based on Fourier analysis of the ED profile. Thus, the molecular-resolution AFM image of the lignoceric-acid monolayer was nondestructively obtained and exhibited a two-dimensional periodic structure with locally disordered molecular arrangements. The image in Figure 7c corresponds to a magnification (3×3 nm^2) of the marked zone shown in Figure 7a. Figure 7c apparently exhibits a discontinuous molecular array in the crystal lattice. That is, a typical edge dislocation can be observed in the center portion of the image, in which an additional molecular array is inserted between two molecular arrays coming down. The direct observation of a crystal defect such as an edge dislocation in the monolayer was made for the first time, resulting from the ability to prepare mechanically stable monolayers.[25]

Figure 8 shows a filtered AFM image with a scan area of 5×5 nm^2 for a stearic-acid crystalline monolayer which was prepared by the multistep creep method. Although scanning was performed repeatedly on the stearic-acid monolayer prepared at a high surface pressure of 23 mN m^{-1} by the multistep creep method, the monolayer was not damaged by the tip. A raised region in the AFM image represents a single methyl group of the stearic-acid molecule in the monolayer. The AFM image indicates that stearic-acid molecules are regularly arranged in a hexagonal array with a (10) spacing of 0.42 nm. This magnitude matches the spacing of 0.42 nm which was estimated from the ED pattern of the stearic-acid monolayer.[22]

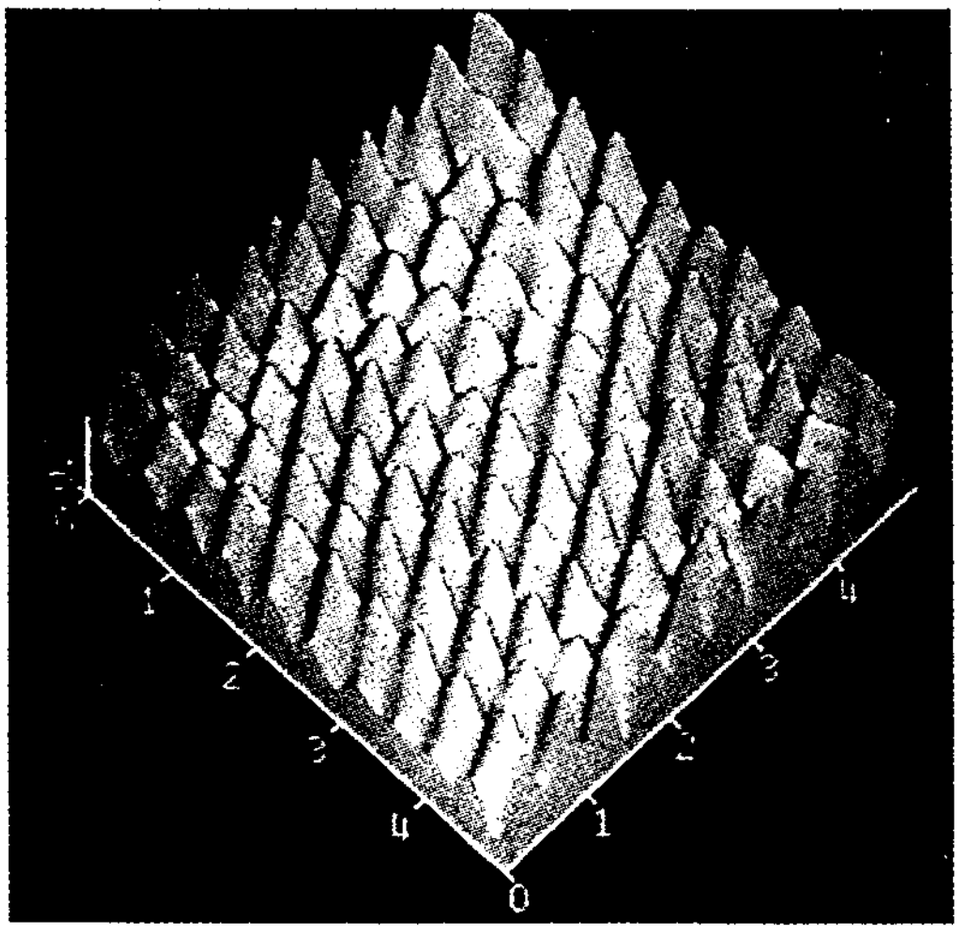

Figure 8. Filtered AFM image of a stearic-acid monolayer on a scan area of 5 × 5 nm^2. The stearic-acid molecules were regularly arranged in a hexagonal array with a (10) spacing of 0.42 nm.

Structural Regularity-Waveguide Property Relationships of LB Films

A fusion-oriented crystalline monolayer of stearic acid was prepared. Stearic-acid monolayers were compressed to a surface pressure of 24 mN m^{-1} at a compression speed of 120 mm^2 s^{-1} by the continuous compression or multistep creep methods.[22] Then, 150 layers were transferred onto the substrate by the vertical dipping method to construct the LB films. The propagation loss of the LB film waveguides was measured on the basis of the scattered light intensities from the waveguide. Light from a He-Ne laser was coupled into the waveguide through the use of a prism.

Figure 9 shows the AFM images for LB films prepared by (a) continuous compression and (b) multistep creep methods on a scan area of 20×20 mm^2. The surface morphology of the LB film prepared by the multistep creep method was fairly homogenous while that of the LB film prepared by the continuous compression method was heterogenous.

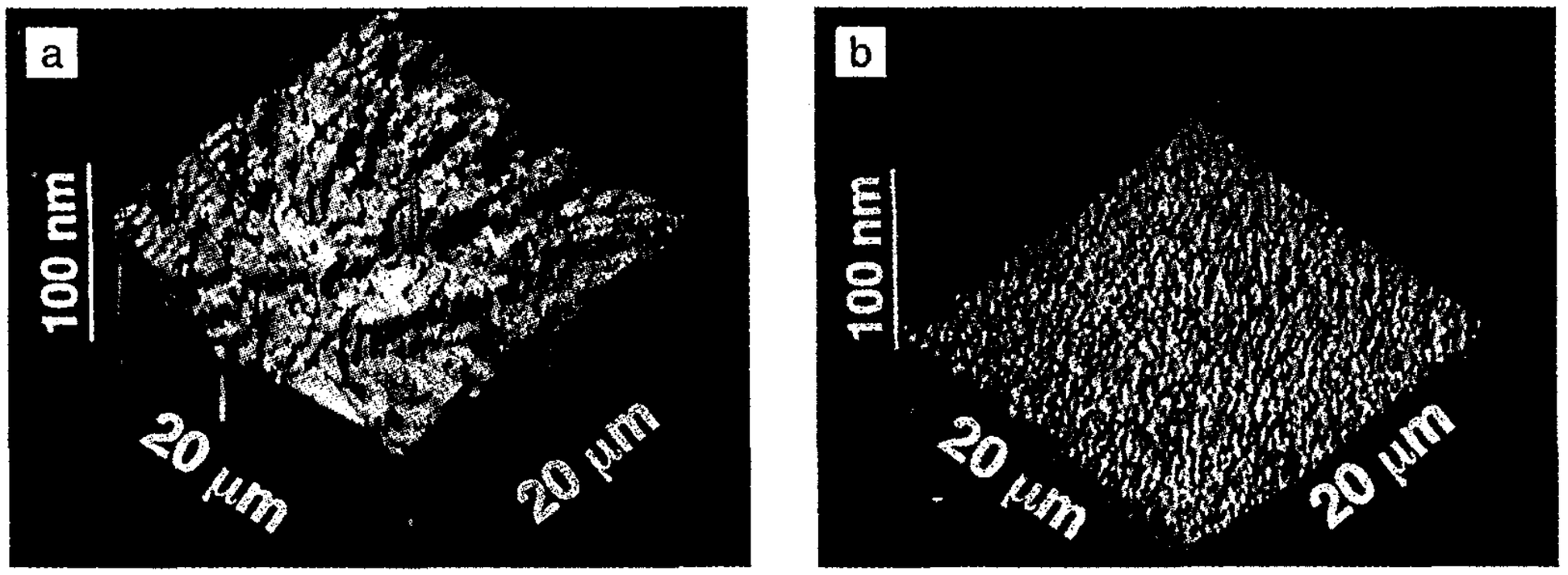

Figure 9. AFM images of LB films composed of monolayers prepared by (a) the continuous compression method and (b) the multistep creep method on a scan area of 20 × 20 μm².

This morphological difference on the top surface of each LB film might be caused by the difference in the preparation processes of monolayers on the water surface. It is reasonable to consider from Figure 9 and Table II that the propagation loss of the LB film waveguide is strongly related to the flatness of the surface morphology of the waveguide. The LB film with a homogenous surface morphology can be constructed by a mechanically stable monolayer being formed with sufficient structural relaxation.[26] The propagation loss of the LB film waveguide was increased by the surface roughness of the LB film. Therefore, the LB film waveguide with a low propagation loss should be composed of monolayers prepared by a structural regularization method such as the multistep creep method.[26]

Table II: Propagation Loss of LB Films Prepared by Continuous Compression and Multistep Creep Methods.

Preparation Method	Propagation Loss $dB \cdot cm^{-1}$
Continuous compression	8.4
Multistep creep	2.5

References

1. T. Kajiyama, Y. Oishi, M. Uchida, N. Morotomi, J. Ishikawa, and Y. Tanimoto, *Bull. Chem. Soc. Jpn.* **65** (1992) p. 864.
2. T. Kajiyama, Y. Oishi, M. Uchida, Y. Tanimoto, and H. Kozuru, *Langmuir* **8** (1992) p. 1,563.
3. N. Uyeda, T. Takenaka, K. Aoyama, M. Matsumoto, and Y. Fijiyoshi, *Nature* **327** (1987) p. 319.
4. D. Hönig, G.A. Overbeck, and D. Möbius, *Adv. Mater.* **4** (1992) p. 419.
5. K. Kjaer, J. Als-Nielsen, C.A. Helm, P. Tippman-Krayer, and H. Möhwald, *J. Phys. Chem.* **93** (4) (1989) p. 3,200.
6. H. Möhwald, *Thin Solid Films* **159** (1988) p. 1.
7. T. Kajiyama, L. Zhang, M. Uchida, Y. Oishi, and A. Takahara, *Langmuir* **9** (1993) p. 760.
8. G.L. Gaines, Jr., *Insoluble Monolayers at Liquid-Gas Interface* (Interscience, New York, 1966).
9. S. Fereshtehkhou, R.D. Neuman, and R. Ovalle, *J. Colloid Interface Sci.* **109** (1986) p. 385.
10. T. Kajiyama, Y. Tanimoto, M. Uchida, Y. Oishi, and R. Takei, *Chem. Lett.* (1989) p. 189.
11. T. Kajiyama, I. Hanada, K. Shuto, and Y. Oishi, *Chem. Lett.* (1989) p. 193.
12. M. Takayanagi and M. Matsuo, *J. Macromol. Sci., Phys.* **B1** (1967) p. 407.
13. T. Kajiyama, T. Okada, A. Sakoda, and M.

Takayanagi, *J. Macromol. Sci., Phys.* **B7** (1973) p. 583.
14. T. Kijima, K. Koga, K. Imada, and M. Takayanagi, *Polym. J.* **7** (1975) p. 14.
15. T. Kijima, K. Koga, K. Imada, and M. Takayanagi, *J. Macromol. Sci. Phys.* **B10** (1974) p. 709.
16. P. Dutta, J.B. Peng, B. Lin, J.B. Ketterson, and M. Prakash, *Phys. Rev. Lett.* **58** (1987) p. 2,228.
17. T. Kajiyama, Y. Oishi, M. Uchida, and Y. Takashima, *Langmuir* **9** (1993) p. 1,978.
18. T. Kajiyama, N. Morotomi, M. Uchida, and Y. Oishi, *Chem. Lett.* (1989) p. 1,047.
19. Y. Oishi, H. Kozuru, K. Shuto, and T. Kajiyama in *Transactions of the Materials Research Society of Japan* (Mater. Res. Soc. Symp. Proc. **15A**, Pittsburgh, 1994) p. 563.
20. D. Hofmann and E. Walenta, *Polymer* **28** (1987) p. 1,298.
21. Y. Oishi, F. Hirose, T. Kuri, and T. Kajiyama, *J. Vac. Sci. Technol. A* **12** (1994) p. 2,971.
22. T. Kuri, F. Hirose, Y. Oishi, and T. Kajiyama, *Rept. Prog. Polym. Phys. Jpn.* **36** (1993) p. 209.
23. T. Kajiyama, Y. Oishi, F. Hirose, K. Shuto and T. Kuri, *Chem. Lett.* (1993) p. 1,121.
24. T. Kajiyama, Y. Oishi, F. Hirose, K. Shuto, and T. Kuri, *Langmuir* **10** (1994) p. 1,297.
25. T. Kajiyama, Y. Oishi, K. Suehiro, F. Hirose, and T. Kuri, *Chem. Lett.* (1995) p. 241.
26. T. Kuri, N. Honda, Y. Oishi, and T. Kajiyama, *Chem. Lett.* (1994) p. 2,223. □